A New Permanent-magnet Vernier In-wheel Motor for Electric Vehicles

Jiangui Li, *Student Member, IEEE*, Diyun Wu, Xiaodong Zhang, Shuang Gao
Department of Electrical and Electronic Engineering, The University of Hong Kong, Hong Kong
Email: jgli@eee.hku.hk

***Abstract*-This paper proposes a new permanent-magnet vernier (PMV) in-wheel motor to meet the new demands arising from electric vehicles (EVs). It can offer the advantages of light weight, compact size and low-speed high-torque operation. The key is to newly introduce the flux-modulation poles (FMPs) which can effectively modulate the high-speed rotating field of the armature windings and the low-speed rotating field of the PM outer-rotor. By using the time-stepping finite element method (TS-FEM), the performance of the proposed machine can be accurately analyzed. In addition, a prototype is constructed to experimentally verify the simulation results.**

I. Introduction

With ever increasing concerns on fossil energy shortage and global warming, there is fast growing interest in electric vehicles (EVs) [1-3]. Up to now, EVs can be classified as three main types: battery EVs [4, 5], fuel cell EVs [6-8] and hybrid EVs [8, 10]. No matter in which type of EVs, electrical motor is fully or partially substituted for internal combustion engine to drive the vehicles. Thus high performance driving motor has become a core technology for EVs.

In early days, induction motors were preferred for EVs due to their high reliability, manufacturing facilitation and low cost [11-13]. Recently, switched reluctance motors have also been recognized to have considerable potential for EVs because of their simple construction and outstanding torque-speed characteristics [14, 15]. With the advent of high-energy permanent magnets (PMs), some kinds of PM motors have been developed to offer higher power density and operating efficiency, such as PM brushless dc motor [16-21], PM axial flux motor [22-24], PM double salient motor [25-29], PM transverse-flux motor [30, 31] and so on. Some hybrid excitation motor drives have also been proposed to enable the maximum power tracking under different operation state [32-39].

It is well known that for certain power rating, higher rated speed implies smaller motor size as well as lighter weight. Thus in most EV systems, the driving motors are designed to be rated at very high speed (4000rpm or above). However, such motors are demanded to offer high-torque low-speed (around 1000 rpm) operation as well as lightweight and compact design generally. Therefore the motor of the in-wheel EVs system still suffers from the well-known matching problem: the modern high-speed (around 4000rpm) motor, which cannot match with the wheel speed (around 1000 rpm) of EVs. Currently, this problem is handled by either adopting a speed-boost planetary gear [40] or using low-speed machine design [41-43]. The former one causes mechanical wear and tear, audible noise and low efficiency, whereas the latter one increases the generator size and weight as well as raw material cost.

Recently, this matching problem has been solved by integrating a coaxial magnetic gear into a permanent-magnet (PM) motor [41, 44], which allows for directly mounting onto the wheel of EVs to operate at lower speeds. However, this kind of magnetic-geared in-wheel motor desires a complex structure, involving two rotating bodies and three airgaps, which increases manufacture difficulty, cost, the associate transmission loss noise, vibration, and regular lubrication. Its simplified version, namely the magnetic-geared machine in [45] also has two airgaps.

It is well known that the vernier effect makes it possible to offer low-speed high-torque operation, while avoiding the increase of the number of armature winding pole-pairs [46. 47]. The venier reluctance machine generally has two types, stator-excitation [48, 49], and rotor-excitation [50]. In order to improve the power density, the vernier reluctance machine incorporates PMs to provide the excitation, thus becoming the PM vernier (PMV) machine [51-56].

This paper presents the design of a new kind of PMV motor for the direct-drive of in-wheel EVs. A PMV in-wheel motor was designed in the form of a permanent-magnet vernier outer-rotor motor. The proposed PMV in-wheel motor was simulated by using time steeping finite element method (TS-FEM) to get the steady state parameters. In Section II, the configuration of the proposed PMV in-wheel motor propulsion system will be introduced and the working principle is illustrated. Section III will be devoted to the mathematical model of the proposed PMV in-wheel machine. In Section IV, the finite element analysis of the proposed machine will be presented and the machine performances will be assessed. Hence, its validity will be verified quantitatively. Finally, conclusion will be drawn in Section V.

II. Principle Of Operation

Fig.1 shows the schemes of the outer-rotor PMV in-wheel motor when it serves as the in-wheel motor drive for EVs, especially for motorcycles. It can be seen that these in-wheel motor drives effectively utilize the outer-rotor nature and is directly coupled with the tire rims. So, this topology can fully utilize the space, hence greatly reducing the size and weight of the drive system for EV applications.

Manuscript received 15 June 2010. Corresponding author: Jiangui Li (e-mail: jgli@eee.hku.hk).
Digital Object Identifier inserted by IEEE

978-1-4244-8218-4/10/$26.00 ©2010 IEEE

By borrowing the concept of magnetic gears and the outer-rotor arrangement of other machines, the proposed PMV in-wheel machine is shown in Fig. 2 and the corresponding prototype is show in Fig. 3. The key is to newly introduce the flux-modulation poles (FMPs) into the outer part of the inner stator, which resemble the ferromagnetic segments of the stationary ring in the coaxial magnetic gear, to modulate the high-speed rotating field of the armature windings and the low-speed rotating field of the PM outer-rotor. Similar to the magnetic gear or other PMV machines, the number of pole-pairs in the space harmonic flux density distribution produced by either the high speed rotating field of the armature winding and the low rotating field of the rotor permanent magnets, is given by:

$$p_r = N_s - p_s \tag{1}$$

where N_s is the number of FMPs, p_r is the number of rotor PM pole-pairs and p_s is the number of armature winding pole-pairs. Consequently, the high-to-low speed ratio G_r is given by:

$$G_r = \frac{|mp_s + kN_s|}{mp_s} \tag{2}$$

where $m = 1,3,\cdots$ and $k = 0,\pm1,\pm2,\cdots$.

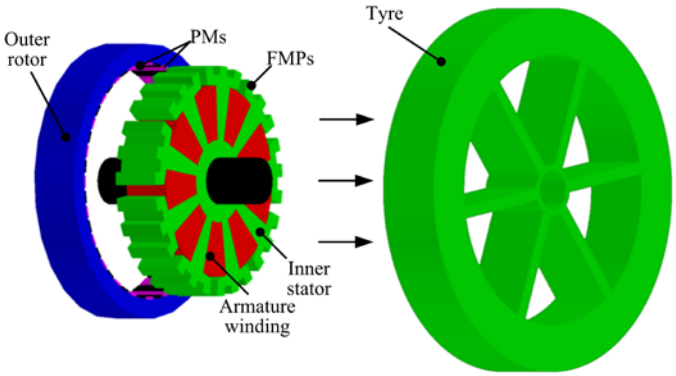

Fig. 1. Scheme of the proposed PMV in-wheel motor system.

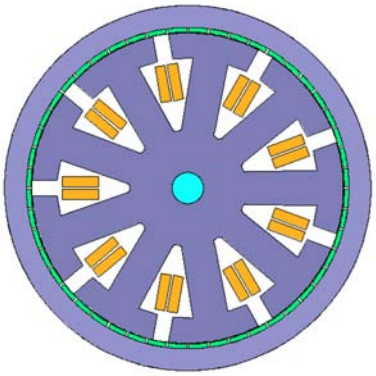

Fig. 2. Proposed PMV in-wheel motor.

In this design, the combination of $m = 1$ and $k = -1$ is selected since it yields the highest asynchronous space harmonic. There are 9 slots in the inner stator, which are occupied by 3-phase armature windings with 6 poles ($p_s = 3$). Each stator tooth is split into 3 FMPs, thus constituting totally 27 FMPs ($N_s = 27$). From (1), $p_r = 24$ is resulted, which denotes that there are 48 PM poles mounting on the outer rotor. From (2), it yields $G_r = -8:1$, namely the rotor speed is only 1/8 of that in the conventional machine with the same number of armature winding pole-pairs and stator slots, but rotating in an opposite direction. Therefore, when the speed of rotating field in the stator is 8000 rpm, the outer rotor speed is scaled down to 1000 rpm.

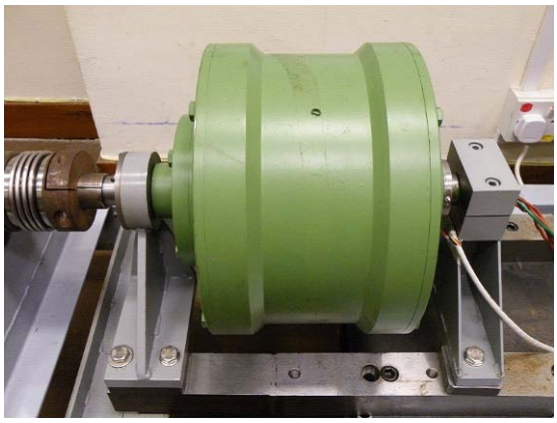

Fig. 3. Prototype of proposed PMV in-wheel motor.

Compared with the previous designs, the proposed machine takes the following advantages:

- This structure involves only one airgap, which is much simpler than the magnetic-geared machine structure (involving three airgaps) [40, 44], and the other PMV machine (involving two airgaps) [46].
- The outer-rotor arrangement inherently provides a large diameter to accommodate a large number of PM poles, and enables full utilization of the inner space for the stator to accommodate the armature windings, thus eliminating the problem of large vacancy in the double excitation PMV machine [46].
- The outer rotor allows for direct coupling with the wheel, which can alleviate the bearing requirements and improving the mechanical integrity.
- The inner-stator arrangement with FMPs enables to adopt compact armature windings, therefore avoiding the problem of drum windings used in [46]. Also, the armature windings adopt the coil pitch equal to the slot pitch, which can minimize the end-windings, hence saving the copper material and reducing the copper loss.

III. Analysis Approach

The TS-FEM is employed to analyze the system performances. It has been verified that it is an efficient way to analyze the motor drives [57]. Firstly, the electromagnetic field equation of the machine is governed by:

$$\Omega: \frac{\partial}{\partial x}\left(\nu\frac{\partial A}{\partial x}\right) + \frac{\partial}{\partial x}\left(\nu\frac{\partial A}{\partial y}\right) = -\frac{i}{S} + \nu\left(-\frac{\partial B_{ry}}{\partial x} + \frac{\partial B_{rx}}{\partial y}\right) + \sigma\frac{\partial A}{\partial t} \tag{3}$$

where Ω is the boundary of calculation, A is the magnetic vector potential component along the z-axis, J is the current density, ν is the reluctivity, σ is the electrical conductivity, B_{rx} and B_{ry} are the remnant flux density components of the PM

along the *x* and *y* axes respectively.

A. In the Airgap and the Iron Cores

The field equation expressed in the 2-D Cartesian coordinates, in regions without source current and PM is

$$\Omega_1 : \frac{\partial}{\partial x}\left(\nu\frac{\partial A}{\partial x}\right)+\frac{\partial}{\partial y}\left(\nu\frac{\partial A}{\partial y}\right)=0 \tag{4}$$

where Ω_1 is the region of the airgap and the iron cores, A is the axial component of the magnetic vector potential, and ν is the reluctivity of the material.

B. In the Stranded Windings

In the armature winding where the current density is uniform, the field equation is

$$\Omega_2 : \frac{\partial}{\partial x}\left(\nu\frac{\partial A}{\partial x}\right)+\frac{\partial}{\partial y}\left(\nu\frac{\partial A}{\partial y}\right)=-\frac{i}{S} \tag{5}$$

where K_w is the polarity (+1 or −1) to represent either the forward paths or return paths, i is the stator phase current, S is the conductor area of each turn of armature winding, and Ω_2 represent the region of forward paths and return paths of the conductor.

C. In the PMs

In the PM region, the total current i_w in each piece of the PM should be zero. The field equation is given by

$$\Omega_3 : \frac{\partial}{\partial x}\left(\nu\frac{\partial A}{\partial x}\right)+\frac{\partial}{\partial y}\left(\nu\frac{\partial A}{\partial y}\right)=\nu\left(-\frac{\partial B_{\mathrm{ry}}}{\partial x}+\frac{\partial B_{\mathrm{rx}}}{\partial y}\right) \tag{6}$$

where Ω_3 is the boundary of the PMs, ν is the reluctivity of the material, B_{rx} and B_{ry} are the *x*-axis and *y*-axis components of the PM remnant flux density respectively.

Secondly, the armature circuit equation of the machine is expressed as [58]:

$$u = Ri + L\frac{di}{dt} + e \tag{7}$$

where i is the stator phase current, R is the stator winding resistance, L is the inductance of the armature windings, S is the sectional area of the conductor of each phase, and u is the branch voltage of the winding. The induce electromotive force (EMF) in the winding is

$$e = -\frac{l}{S}\iint_{\Omega^+}\frac{\partial A}{\partial t}d\Omega+\frac{l_e}{S}\iint_{\Omega^-}\frac{\partial A}{\partial t}d\Omega \tag{8}$$

If (5) and (7) are directly coupled together, the coefficient matrix of the system equations will become asymmetrical in the nodal analysis [58, 59]. Consequently, an additional unknown in the stranded windings is proposed below in order to make the coefficient matrix symmetrical.

Using the backward Euler's method [60] to discretize the time variable, one gets

$$\frac{di^k}{dt}=\frac{i^k-i^{k-1}}{\Delta t} \tag{9}$$

where, the superscript k is the step number in the time stepping process, i^k is the stator phase current in the k th step, and the step size $\Delta t = t^k - t^{k-1}$. Substituting the above equation into (7), one has

$$i^k=\left(-e-L\frac{\Delta i^k}{\Delta t}+u\right)\Big/\left(R+\frac{L}{\Delta t}\right) \tag{10}$$

Substituting (10) into (7), the field equation is

$$\begin{aligned}&\frac{\partial}{\partial x}\left(\nu\frac{\partial A}{\partial x}\right)+\frac{\partial}{\partial y}\left(\nu\frac{\partial A}{\partial y}\right)+\frac{l}{S\left(R+\frac{L}{\Delta t}\right)}e-\frac{l}{S\left(R+\frac{L}{\Delta t}\right)}u\\&=\frac{l}{S\left(R+\frac{L}{\Delta t}\right)}\frac{L}{\Delta t}i^{k-1}\end{aligned} \tag{11}$$

Then substituting (8) and (10) into (7), the branch equation is

$$\frac{l}{S\left(R+\frac{L}{\Delta t}\right)}\iint_{\Omega}\frac{\partial A}{\partial t}d\Omega+\frac{1}{\left(R+\frac{L}{\Delta t}\right)}u=i^k-\frac{L}{\Delta t\left(R+\frac{L}{\Delta t}\right)}i^{k-1} \tag{12}$$

Equation (8) can also be written as,

$$\frac{l}{S\left(R+\frac{L}{\Delta t}\right)}\iint_{\Omega}\frac{\partial A}{\partial t}d\Omega+\frac{1}{\left(R+\frac{L}{\Delta t}\right)}e=0 \tag{13}$$

Thirdly, the motion equation is given by:

$$\frac{l}{\mu_0}\oint r^2 B_r B_t d\theta = T + J\frac{d\omega}{dt}+B\omega \tag{14}$$

where J is the moment of inertia, ω is the rotor speed, T is the mechanical driving torque, T_e is the electromagnetic torque, and B is the damping coefficient.

By coupling the field equation (3), voltage equation (7) and the motion equation (14), the TS-FEM can be performed to calculate both the steady-state and dynamic performances of the motor.

IV. Performances of The Proposed Machine

In order to illustrate the validity of the proposed machine, its performances are quantitatively analyzed by TS-FEM. The overall outside diameters, axial lengths, total copper volume and PM volume are listed in Table I. It can be found that the proposed machine possesses the large rated power and low rated speed for directly driving in-wheel EVs. This merit is actually due to the proposed PMV structure which can significantly improve the power density.

TABLE I

Design Data Of The PMV In-Wheel Machine

Items	Rated values
Rated power	1.6 kW
Rated phase voltage	110 V
Rated current	9 A
Rated speed	1000 rpm
Gear ratio	−8 : 1
No. of armature winding poles	6
No. of stator poles	9
No. of FMPs	27
No. of rotor poles	48
Overall outside diameter	240 mm
Shaft diameter	35 mm
Axial length	60 mm

Fig. 4 shows the magnetic field distributions of the proposed machine under no-load. It can be observed that the flux lines per stator tooth of the proposed machine can pass through the FMPs separately, hence verifying the desired flux modulation. Furthermore, the flux lines concentrated in six poles so that the output torque is more effective.

The airgap flux density waveforms are shown in Fig. 5. From the figure, the averaged peak value of the proposed machine is 0.856 T and the maximum value is 1.015 T, quantitatively. It also can be seen that the proposed machine has 24 pole-pairs in the airgap within 360° which corresponds to 24 pole-pairs of the PMs on the rotor, thus well agreeing with each other. In addition, there are several peaks that have higher amplitudes then others as marked in the figure. This is because at some points, the N poles or S poles happens to face or nearly face the FMPs on the stator, while at some other points, the PM poles happen to object to the stator slots.

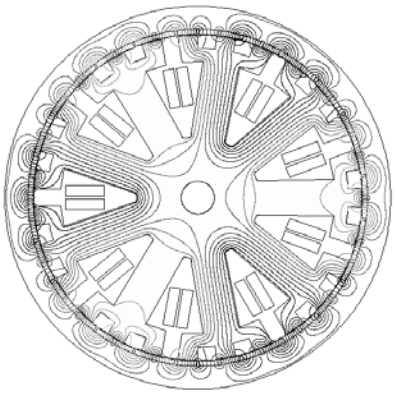

Fig. 4. No-load magnetic field distributions.

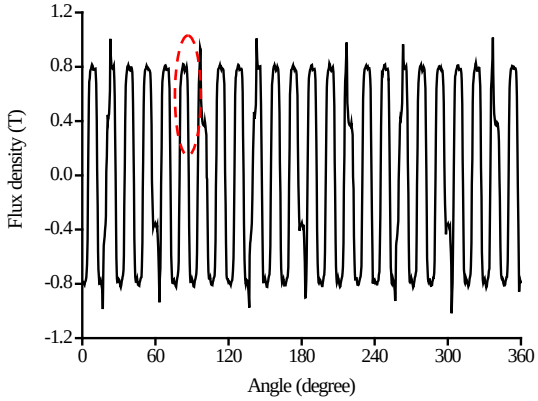

Fig. 5. No-load airgap flux density waveforms.

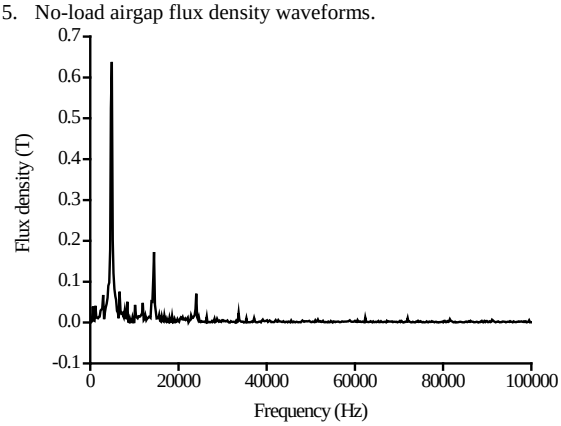

Fig. 6. Harmonic spectra of no-load airgap flux density.

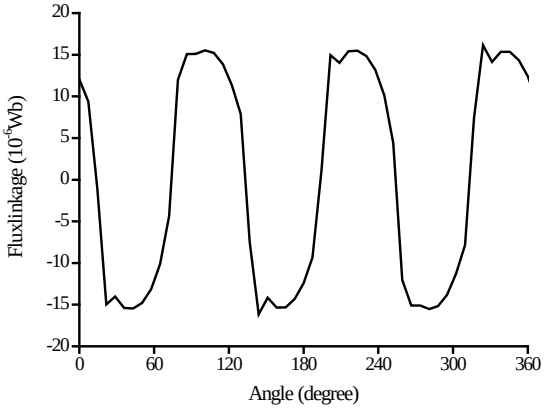

Fig. 7. Resultant magnetic flux linkage.

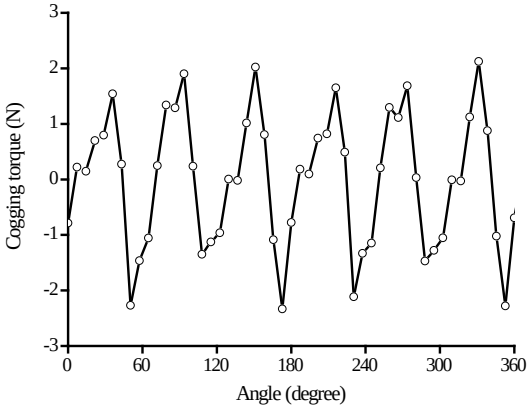

Fig. 8. Cogging torque owing to the structure.

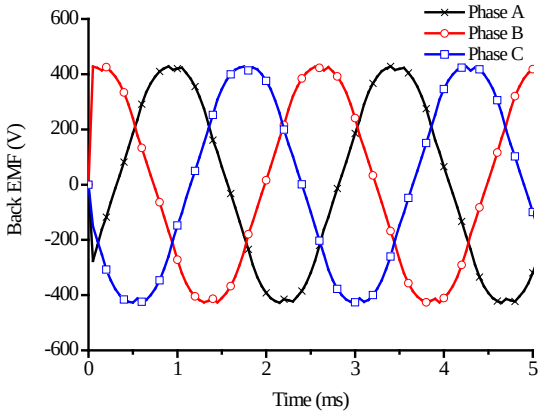

Fig. 9. Back EMF waveforms.

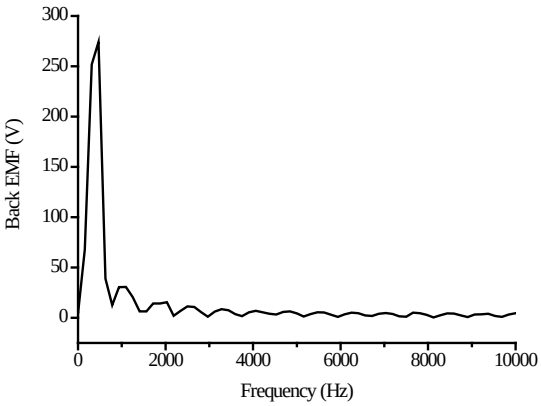

Fig. 10. Harmonic spectra of back EMF.

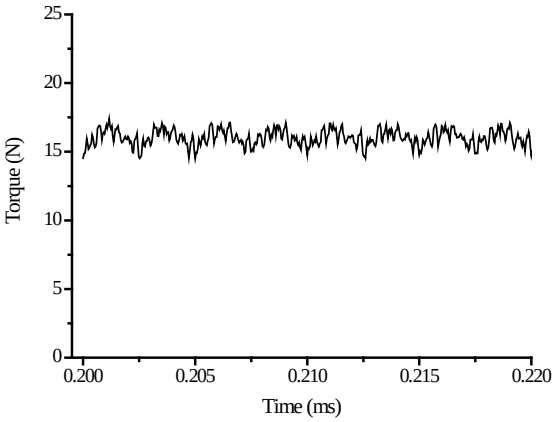

Fig. 11. Steady state torque.

Fig. 6 shows the corresponding harmonic spectra of no-load airgap flux density. The fundamental frequency that works to generate the flux linkage in the airgap is the base frequency 400Hz. And it can be seen from Fig.6 that the amplitude of the harmonics that are 'useless' very small. Fig. 7 shows the resultant magnetic flux linkage in no-load analysis. From the figure, there are 3 pole-pairs of the flux linkage, which are corresponding to the 3 pole-pairs of the armature winding. Furthermore, it indicated that the number of the pole-pairs of the airgap flux density (Fig. 5) is 8 times of the number of the pole-pairs of the resultant flux linkage in 360° mechanical degrees, which validities the gear ratio of this design. Fig. 8 shows the cogging torque generated due to the different magnetic resistance of difference path generated by the pole-pitch structure of the proposed PMV in-wheel motor. The maximum cogging torque is 2.163 N and the average value is 1.829 N, taking up 13.5% and 11.4% respectively. However, this data is acceptable according to the experience of previous work.

Fig. 9 shows the back EMF waveforms of the proposed PMV in-wheel motor at the rated speed of 1000 rpm. It can be found that the root mean square (RMS) value of the proposed machine is 427.66 V. Fig. 10 shows the corresponding harmonic spectra of the back EMF, it can be observed that the no-load EMF waveform of the proposed machine is very sinusoidal. The base frequency is 400 Hz and the harmonics are mainly generated by the FMPs. Fig. 11 shows steady state torque at rated speed. The average output torque is 16.011 N. Due to the use of PMs, the PMV in-wheel motor can definitely produce high torque while operating at low rotational speed. This characteristic can benefit to the application of direct-drive in-wheel EVs.

V. Conclusion

In this paper, a novel PMV in-wheel machine has been developed for direct-drive EVs, which can offer low-speed operation to directly coupled into the wheel, and enable high-speed rotating field design to maximize the power density. Compared with its mechanical gear counterpart, the proposed machine can eliminate the mechanical wear and tear as well as transmission loss, thus improving the generation reliability and efficiency. Compared with its PMV counterparts, it offers higher power density and higher output voltage, while reducing the raw material volume and hence the overall cost. By using the TS-FEM, the proposed machine is quantitatively analized in terms of back EMF generation and torque-handling capability, thus verifying that it is very promising for direct-drive application in EVs.

Acknowledgment

This work was supported by a grant (Project No. HKU7105/07E) from the Hong Kong Research Grants Council, Hong Kong Special Administrative Region, China.

References

[1] C. C. Chan and K. T. Chau, *Modern Electric Vehicle Technology*, Oxford University Press, 2001.

[2] K. T. Chau and Y. S. Wong, "Overview of power management in hybrid electric vehicles," *Energy Conversion and Management*, vol. 43, no. 15, June 2002, pp. 1953-1968.

[3] O. D.Momoh, M. O. Omoigui, "An overview of hybrid electric vehicle technology," *Vehicle Power and Propulsion Conference*, 2009, pp.1286-1292.

[4] C. C. Chan and K. T. Chau, "An advanced permanent magnet motor drive system for battery-powered electric vehicles," *IEEE Transactions on Vehicular Technology*, vol. 45, no. 1, 1996, pp. 180-188.

[5] G. Gutmann, "Applications-transportation, electric vehicle: batteries," *Encyclopedia of Electrochemical Power Sources*, 2009, pp. 219-235.

[6] D. Tokumura, Y Horii, J Watanabe, "Fuel cell electric vehicle," US Patent App. 11/199,156, 2005.

[7] L. Pino, A. Vita, M. Cordaro, V. Recupero, and M. S. Hegde, **"**A comparative study of Pt /CeO_2 catalysts for catalytic partial oxidation of methane to syngas for application in fuel cell electric vehicles," *Applied Catalysis A*: General 243, 2003, pp. 135-146.

[8] K. M. Rahman, N. R. Patel, T. G. Ward, J. M. Nagashima, F. Caricchi, and F. Crescimbini, "Application of direct-drive wheel motor for fuel cell electric and hybrid electric vehicle propulsion system," *IEEE Trans. Industry Applications*, vol. 42, no. 5, 2006, pp.1185 – 1192.

[9] K. T. Chau, C. C. Chan and C. Liu, "Overview of permanent-magnet brushless drives for electric and hybrid electric vehicles," *IEEE Transactions on Industrial Electronics*, vol. 55, no. 6, June 2008, pp. 2246-2257.

[10] K. T. Chau and C. C. Chan, "Emerging energy-efficient technologies for hybrid electric vehicles," *Proceeding of IEEE*, vol. 95, no. 4, pp.821-835, 2007.

[11] J. O. P. Pinto, B. K. Bose and L. E. B. da Silva, "A stator-flux-oriented vector-controlled induction motor drive with space-vector PWM and flux-vect synthesis by neural networks," *IEEE Transactions on Industry Application*, vol. 37, no. 5, pp.1308-1318.

[12] C. C. Chan, L. Yan, P. Chen, Z. Wang and K. T. Chau, "Analysis of electromagnetic and thermal fields for induction motors during starting," *IEEE Transactions on Energy Conversion*, vol. 9, no. 1, March 1994, pp. 53-60.

[13] D. H. Cho, H. K. Jung, C. G. Lee, "Induction motor design for electric vehicle using a niching genetic algorithm," *IEEE transactions on industry applications*, 2001, pp.994-999.

[14] K. M. Rahman, B. Fahimi, G. Suresh, A. V. Rajarathnam, and M. Ehsani, "Advantages of switched reluctance motor applications to EV and HEV: design and control issues," *IEEE Transactions on Industrial Application*, vol. 36, 2000, pp.111-121.

[15] Y. J. Zhan, C. C. Chan, and K. T. Chau, "A novel sliding mode observer for indirect position sensing of switched reluctance motor drives," *IEEE Transactions on Industrial Electronics*, vol. 46, no. 2, April 1999, pp. 390-397.

[16] K. T. Chau, D. Zhang, J. Z. Jiang, C. Liu and Y. J. Zhang, "Design of a magnetic-geared outer-rotor permanent-magnet brushless motor for electric vehicles," *IEEE Transactions on Magnetics*, vol. 43, no. 6, June 2007, pp. 2504-2506.

[17] J. Gan, K. T. Chau, C. C. Chan and J. Z. Jiang, "A new surface-inset, permanent-magnet, brushless DC motor drive for electric vehicles," *IEEE Transactions on Magnetics*, vol. 36, no. 5, September 2000, pp. 3810-3818.

[18] P. Zheng, Y. Liu, Y. Wang, and S. K. Cheng, "Magnetization analysis of the brushless DC motor used for hybrid electric vehicle," *IEEE Transactions on Magnetics*, vol. 41, no. 1 (2), 2005, pp. 522-524.

[19] K. T. Chau, W. Cui, J. Z. Jiang and Z. Wang, "Design of permanent magnet brushless motors with asymmetric air gap for electric vehicles," *Journal of Applied Physics*, vol. 99, no. 8, April 2006, paper no. 80R322, pp. 1-3.

[20] C. Yu, K. T. Chau, X. Liu and J. Z. Jiang, "A flux-mnemonic permanent magnet brushless motor for electric vehicles," *Journal of Applied Physics*, vol. 103, no. 7, 2008, pp. 1-3.

[21] Y. Wang, K. T. Chau, C. C. Chan and J. Z. Jiang, "Design and analysis of a new multiphase polygonal-winding permanent-magnet brushless dc machine," *IEEE Transactions on Magnetics*, vol. 38, no. 5, September 2002, pp. 3258-3260.

[22] P. R. Johansen, D. Patterson, C. O'Keefe, and J. Swenson, "The use of an axial flux permanent magnet in-wheel direct drive in an electric bicycle," *Renewable Energy*, vol. 22, no. 1-3, 2001, pp. 151-157.

[23] F. Caricchi, F. Crescimbini, F. Mezzetti, and E. Santini, "Multistage axial-flux PM machine for wheel direct drive," *IEEE Transactions on Industry Applications*, vol. 32 , no. 4, 1996, pp.882–888.

[24] P. Zheng, J. Zhao, R. Liu, C. Tong, Q. Wu, "Magnetic characteristics investigation of an axial-axial flux compound-structure PMSM used for HEVs," *IEEE Transactions on Magnetics*, vol. 46, no. 6, 2010, pp. 2191-2194.

[25] M. Cheng, K. T. Chau and C. C. Chan, "New split-winding doubly salient permanent magnet motor drive," *IEEE Transactions on Aerospace and Electronic Systems*, vol. 39, no. 1, January 2003, pp. 202-210.

[26] K. T. Chau, Q. Sun, Y. Fan and M. Cheng, "Torque ripple minimization of doubly salient permanent magnet motors," *IEEE Transactions on Energy Conversion*, vol. 20, no. 2, June 2005, pp. 352-358.

[27] K. T. Chau, M. Cheng, and C. C. Chan, "Performance analysis of 8/6-pole doubly salient permanent magnet motor," *Electric Machines and Power Systems*, vol. 27, no. 10, October 1999, pp. 1055-1067.

[28] M. Cheng, K. T. Chau, C. C. Chan, and E. Zhou, "Performance analysis of split-winding doubly salient permanent magnet motor for wide speed operation," *Electric Machines and Power Systems*, vol. 28, no. 3, March 2000, pp. 277-288.

[29] M. Cheng, K. T. Chau and C. C. Chan, "Static characteristics of a new doubly salient permanent magnet motor," *IEEE Transactions on Energy Conversion*, vol. 16, no. 1, March 2001, pp. 20-25.

[30] G. Henneberger, and M. Bork, "Development of a new transverse flux motor," IEE Colloquium on New Topologies for Permanent Magnet Machines, 1997, pp.1-6.

[31] J. K. Wang, K. T. Chau, J. Z. Jiang and C. Yu, "Design and analysis of a transverse flux permanent magnet machine using three dimensional scalar magnetic potential finite element method," *Journal of Applied Physics*, vol. 103, no. 7, pp. 1-3, 2008.

[32] K. T. Chau, Y. B. Li, J. Z. Jiang and C. Liu, "Design and analysis of a stator-doubly-fed doubly-salient permanent-magnet machine for automotive engines," *IEEE Transactions on Magnetics*, vol. 42, no. 10, October 2006, pp. 3470-3472.

[33] M. Cheng, Y. Fan and K. T. Chau, "Design and analysis of a novel stator-doubly-fed doubly salient motor for electric vehicles," *Journal of Applied Physics*, vol. 97, no. 10, May 2005, paper no. 10Q508, pp. 1-3.

[34] K. T. Chau and Z. Wang, "Design of permanent magnets to chaoize doubly salient PM motors for electric compaction," *Journal of Applied Physics*, vol. 99, no. 8, April 2006, paper no. 80R306, pp. 1-3.

[35] M. Cheng, K. T. Chau, and C. C. Chan, "Design and analysis of a new doubly salient permanent magnet motor," *IEEE Transactions on Magnetics*, vol. 37, no. 4, July 2001, pp. 3012-3020.

[36] Y. Fan and K. T. Chau, "Design, modeling, and analysis of a brushless doubly fed doubly salient machine for electric vehicles," *IEEE Transactions on Industry Applications*, vol. 44, no. 3, pp. 727-734. 2008.

[37] K. T. Chau, J. Z Jiang and Y. Wang, "A novel stator doubly fed doubly salient permanent magnet brushless machine," *IEEE Transactions on Magnetics*, vol. 39, no. 5, September 2003, pp. 3001-3003.

[38] K. T. Chau, M. Cheng and C. C. Chan, "Nonlinear magnetic circuit analysis for a novel stator-doubly-fed doubly-salient machine," *IEEE Transactions on Magnetics*, vol. 38, no. 5, September 2002, pp. 2382-2384.

[39] Y. Gong, K. T. Chau, J. Z. Jiang, C. Yu, and W. Li, "Design of doubly salient permanent magnet motors with minimum torque ripple," *IEEE Trans. Magnetics*, vol. 45, no. 10, 2009, pp. 4704-4707.

[40] L. Jian and K. T. Chau, "Design and Analysis of an integrated Halbach-magnetic-geared permanent-magnet motor for electric vehicles," *Journal of Asian Electric Vehicles*, vol. 7, no.1, 2009, pp. 1213-1219.

[41] K. M. Rahman, N. R. Patel, T. G. Ward, J. M. Nagashima, F. Caricchi, and F. Crescimbini, "Application of direct-drive wheel motor for fuel cell electric and hybrid electric vehicle propulsion system," *IEEE Transactions on Industry Applications*, vol. 42, no. 5, 2006, pp. 1185–1192.

[42] G. L. Tao; Z. Y. Ma; L. B. Zhou and L. R. Li; "A novel driving and control system for direct-wheel-driven electric vehicle," *IEEE Transactions on Magnetics*, vol. 41, no. 1 (2) , 2005, pp. 497–500.

[43] C. Liu, K. T. Chau, J. Z. Jiang and S. Niu, "Comparison of stator-permanent-magnet brushless machines," *IEEE Transactions on Magnetics*, vol. 44, no. 11, Nov. 2008, pp. 4405-4408.

[44] L. Jian, K. T. Chau and J. Z Jiang, "An integrated magnetic-geared permanent-magnet in-wheel motor drive for electric vehicles," *IEEE Vehicle Power and Propulsion Conference*, Harbin, China, Sep. 2008, paper no. H08345, pp. 1-6.

[45] L. L. Wang, J.X. Shen, Y. Wang, and, K. Wang, "A novel magnetic-geared outer-rotor permanent-magnet brushless motor," *4th IET Conference on Power Electronics*, 2008, pp. 33-36.

[46] A. Toba, and T. A. Lipo, "Generic torque-maximizing design methodology of surface permanent-magnet vernier machine," *IEEE Trans. on Industry Appl.*, vol. 36, no. 6, 2000, pp. 1539-1546.

[47] A. Toba, and T. A. Lipo, "Novel dual-excitation permanent magnet vernier machine," in *Conf. Rec. IEEE-IAS Annu. Meeting*, 1999, pp. 2539-2544.

[48] S. Taïbi, A. Tounzi, and F. Piriou, "Study of a stator current excited vernier reluctance machine," *IEEE Transactions on Energy Conversion*, vol.21, no.4, 2006, pp.823-831.

[49] D. J. Rhodes, "Assessment of vernier motor design using generalized machine concepts," *IEEE Trans. Power Apparatus and Systems*, vol. PAS-96, no.4, July/August 1977.

[50] A. Tounzi, B. Ramdane, M.E. Zaim, "Study of a rotor current excited vernier reluctance machine," International Conference on Electrical Machines, 2008,pp. 1-6.

[51] E. Spooner, P. Tavner, M. A. Mueller, P. R. M. Brooking, and N. J. Baker, "Vernier Hybrid Machine for Compact Drive Applications," *Second International Conference on Power Electronics*, vol. 1, 31 March-2 April 2004, pp.452 - 457.

[52] E. Spooner and L. Haydock, "Vernier hybrid machines," *IEE Proceeding of Electric Power Application*, vol. 150, no. 6, Nov. 2003.

[53] A. Ishizaki, T. Tanaka, K. Takasaki, and S. Nishikata, "Theory and Optimum Design of PM Vernier Motor," *IEE Conference, Electrical Machines and Drives*, 11-13 Sep. 1995, pp.208-212.

[54] H. Suda, and Y. Anazawa, "Torque analysis of HB-type vernier motor," *IEEE International Conference, Electric Machines & Drives Conference*, vol. 1, 3-5 May 2007, pp.709–714.

[55] J. Jac, D. Matt, N. Ziegler, P. Enrici, and T. Martiré, "Electromagnetic actuator with high torque mass ratio. permanent magnet machine with synchronous and vernier double effect. Application to Aeronautical systems," *International Aegean Conference on Electrical Machines and Power Electronics*, 10-12 Sept. 2007, pp.81–86.

[56] M. A. Mueller and N. J. Baker, "Modelling the performance of the vernier machine," *IEE Proc. Electr, Power Appl.*, vol. 150, no.6, Nov. 2003.

[57] Y. B. Li, S. L Ho, W. N. Fu, W. Y. Liu, "An Interpolative Finite-Element Modeling and the Starting Process Simulation of a Large Solid Pole Synchronous Machine," *IEEE Transactions on Magnetics*, vol. 45, 2009, pp. 4605-4608.

[58] Y. Wang, K. T. Chau, C. C. Chan, and J.Z. Jiang, "Transient analysis of a new outer-rotor permanent-magnet brushless dc drive using circuit-field-torque time-stepping finite element method," *IEEE Transactions on Magnetics*, vol. 38, no. 2, March 2002, pp. 1297-1300.

[59] W. N. Fu, S. L. Ho, H. L. Li, And H. C. Wong, "A multislice coupled finite-element method with uneven slice length division for the simulation study of electric machines," *IEEE Trans. Magnetics*, vol.39, no. 3, 2003, pp.1566-1569.

[60] W.N. Fu, P. Zhou, D. Lin, S. Stanton, Z.J. Cendes, "Modeling of solid conductors in 2-D transient finite element analysis and its application to electric machines," *IEEE International Electric Machines and Drives Conference*, vol. 2,2003, pp. 1272–1278.